Single-electron tunneling in metal droplets in the high conductance regime

S. T. Ruggiero,[1,*] T. B. Ekkens,[1] and Sh. Farhangfar[2]
[1]*University of Notre Dame, Notre Dame, Indiana 46556*
[2]*Department of Physics, University of Jyväskylä, P.O. Box 35 (Y5), FIN-40351 Jyväskylä, Finland*
(Received 27 June 2000; revised manuscript received 24 January 2001; published 10 April 2001)

We present single-electron tunneling results for well-characterized multidroplet systems in the high conductance regime. The work was conducted with tunnel systems comprising ultra-small Ni droplets. The conductance associated with individual droplets was estimated to reach $18-19\,G_K$ in systems exhibiting especially high conductance. The $P(E)$ (phase correlation) theory has been successfully applied to the conductance characteristics of these systems. Our results suggest that in the high conductance regime the droplets can be modeled as single, resistively isolated tunnel junctions. Based on an analysis of the single-electron properties of these systems, the average number of droplets N contributing to the total tunneling conductance can be estimated. For samples in the low conductance regime, it appears that $N=1$, whereas for samples in the high conductance regime $100<N<1000$.

DOI: 10.1103/PhysRevB.63.195405 PACS number(s): 73.23.Hk, 73.40.Gk, 73.40.Rw

I. INTRODUCTION

Coulomb blockade effects associated with tunneling into isolated mesoscopic droplets and dots are now of wide interest. While single-electron tunneling (SET) phenomenology is well understood in the low-tunneling conductance regime, $G \ll G_K \equiv e^2/h$,[1–4] lately the significant consequences of increasing the conductance beyond this regime are being explored in systems such as single-electron transistors,[5] quantum dots,[6] and in small tunnel junctions with[7] and without[8,9] metallic islands.

The present paper looks at multiple-droplet single-electron systems in the high conductance regime. The junctions contained ultra-small Ni droplets (small, isolated islands of Ni metal) with diameters in the range of 1 to 2 nm. The average tunnel conductance G_D of the individual droplets comprising these tunnel systems was as high as $18-19\,G_K$. This is in the regime of the highest tunneling conductances yet studied.[9] We have found that the detailed tunnel characteristics of our high conductance systems can be well-described by the $P(E)$ (phase correlation) theory. This theory considers the effect of the electromagnetic environment on tunneling[10,11] and has been considered for the case of strong tunneling.[9,12–15] We will show that our results for the increase in effective capacitance with tunneling conductance are generally consistent with theoretical results in the range $0<G\lesssim 20\,G_K$. The successful application of the $P(E)$ theory for droplets in the high conductance regime suggests they behave as resistively coupled single junctions rather than double junctions, as is the case in the low conductance regime. In addition, our results allow for a self-consistent estimate of the average number of droplets N participating in the tunneling, which has been absent from previous work, and provides for an estimate of the average conductance associated with individual droplets.

A key issue in these studies is the effective capacitance of the droplets as a function of tunneling conductance. For an island that is decoupled from the environment (as in the case of low tunneling conductance), the effective capacitance C_0 of the island will be determined solely by its geometry and dielectric environment. As coupling to the environment increases (for higher tunneling conductance) the effective capacitance C of the island will increase. To quantitatively study this process in our systems, we have derived the effective droplet capacitance in three independent ways: (1) measurement of the Coulomb-blockade energy, (2) measurement of the thermal activation energy, and (3) fits of tunnel conductance data with $P(E)$ theory. All three measurements were found to be in excellent agreement. With these results in hand, the number of tunneling droplets and a model for the coupling of droplets to the external environment have been established.

II. EXPERIMENT

Our junction preparation method was similar to previous work with ''soft'' metals such as Ag, Au, Cu, In, Pb, etc.,[16,17] which consistently show Coulomb staircase and/or Coulomb blockade effects. As sketched in Fig. 1, tunnel systems used in this paper were of the form: $Al/Al_2O_3/Ni$ droplets$/Al_2O_3/Ag$. The first Al_2O_3 barrier was created by exposing a 100 nm base Al layer to air. This was followed by a 1–5 nm layer of Ni. A second barrier was created by depositing a 1.1–1.2 nm layer of Al *in situ* on top of the thermally evaporated layer of Ni (droplets) and re-exposing the

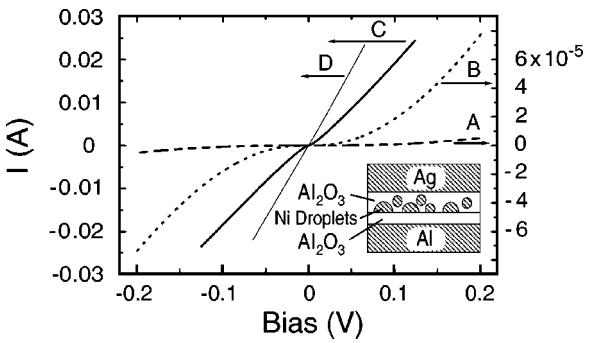

FIG. 1. Geometry and tunneling characteristics of Ni droplet tunnel junctions. Data were taken at 4.2 K.

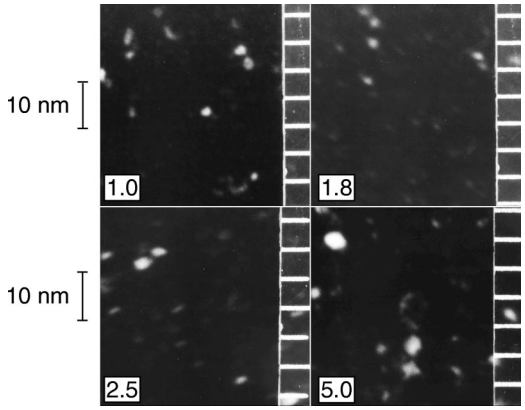

FIG. 2. Scanning transmission electron micrographs of Ni droplet films produced at the same time as films incorporated into tunnel structures. Micrographs for film depositions of 1.0, 1.8, 2.5 and 5.0 nm of Ni are shown, associated with samples *A*, *B*, *C*, and *D*, respectively. Top and bottom size bars refer to top two and bottom two images, respectively.

system to air. Finally, the system was returned to vacuum to receive a 100 nm Ag counter electrode.

III. GENERAL CHARACTERISTICS

The deposition of Ni in the 1–5 nm thickness range resulted in the formation of Ni droplets as shown in Fig. 2. The droplets are isolated islands of Ni metal that coalesce during the evaporation process. The individual images collected here are smaller segments of larger format scanning transmission electron micrographs of films of a given thickness made at the same time as those incorporated into tunnel structures. The bright spots are images of isolated islands of Ni metal. We note that soft metal systems (such as Ag, Au, Cu, In, Pb, etc.) typically coalesce into polycrystalline droplets roughly hemispherical in shape. While detailed crystallographic data are not available for our Ni droplets, the micrographs of these films clearly indicate the presence of isolated islands of Ni, and are similar in general appearance to micrographs of soft metal droplets in a comparable size range.

The associated droplet-size distribution for each Ni deposition thickness is shown in Fig. 3. While it is clear that not all droplets will contribute to the total tunneling conductance of a given multi-droplet tunnel system, it has been observed that the distribution of droplet sizes represented in a given micrograph correlates well with the distribution of droplet sizes predicted on the basis of observed single-electron conductance peaks.[17] It could thereby be concluded that a droplet-size histogram is a fair representation of the distribution of droplets of a given diameter that will contribute to the total tunneling conductance, even though only a small fraction of the total number of droplets physically present in a system will ultimately carry a significant tunneling current. We note that even in the case of sample A—for which we will ultimately conclude that only on the order of a single droplet contributes to the tunnel conductance—the expected blockade energy E_0 associated with a droplet of the mean

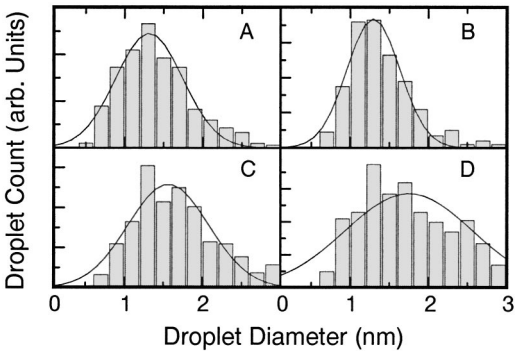

FIG. 3. Histogram and Gaussian fit for each Ni deposition. Samples *A*, *B*, *C*, and *D* correspond to Ni deposition thicknesses of 1.0, 1.8, 2.5, and 5.0 nm, respectively. These films contain droplets with average diameters of 1.3, 1.3, 1.6, and 1.7 nm, respectively.

size as derived from a Gaussian fit to the droplet-size distribution is in good accord with the measured value of the blockade energy E_g.

We do see, however, that there are some differences in Ni droplet formation compared to other metals. The size distributions for our Ni droplets are close to Gaussian (although significant deviations from Gaussian behavior appear to occur as film thickness increases). Although the distributions are not unusual in this regard, they are different with respect to droplet formation in other metals such as Ag, Au, Cu, Pb, etc. For these metals, it is generally observed that the mean droplet diameter is close to the nominal deposition thickness. That is, for films less than ~8 nm in thickness, droplets will form with a mean diameter comparable to the deposited film thickness. However, for Ni droplets, the mean diameter was only a weak function of deposition thickness. For Ni depositions of 1.0, 1.8, 2.5, and 5.0 nm, the mean droplet diameter was 1.3, 1.3, 1.6, and 1.7 nm, respectively. A second difference is the presence of a broad distribution width in Ni droplet diameter. Typical Ag films in the thickness regime considered here have a distribution width σ in the vicinity of 20% of the mean droplet diameter.[16,18] In the case of our Ni droplets σ is significantly larger, ~100% of the mean droplet diameter. A general discussion of metal droplet formation in thin films is given by Pashley *et al.*[19]

In spite of the above-noted differences in the characteristics of Ni droplet layers, they have been successfully used for single-electron studies. Indeed, junctions prepared with Ni droplets have the advantage that if a series of tunnel systems is prepared with increasing Ni deposition thickness, the result is a series of samples with similar average Ni droplet size and increasing tunnel conductance. This has allowed for a more controlled study of the effects of tunnel conductance.

Shown in Fig. 1 are the current-voltage characteristics for the tunnel systems studied. Gaplike structure associated with single-electron tunneling in the Ni droplets is clearly evident as an offset in the quasilinear portion of the characteristics about zero bias. The magnitude of this gap clearly decreases with increasing junction conductance, from samples *A* to *D*, although a Coulomb gap persists for all samples. This can be seen in the $G(V)$ characteristics, Fig. 4, in which gaplike structure is clearly evident for all junctions.

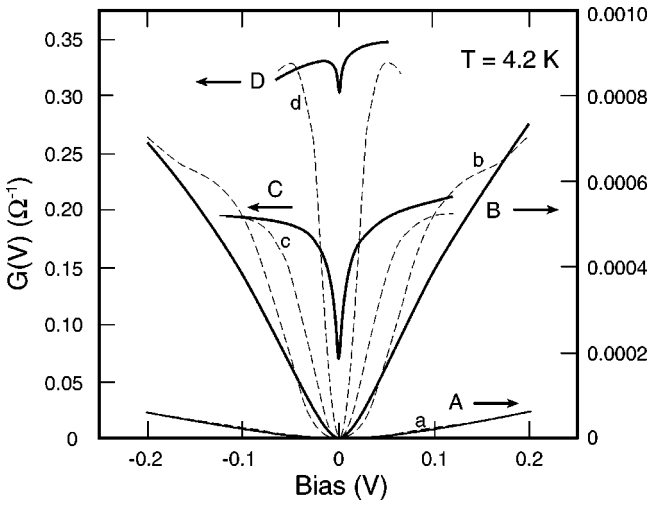

FIG. 4. Tunneling conductance $G(V) \equiv dI/dV$ for all junctions studied. The dashed lines are fits to the data using standard semiclassical SET theory. The fit associated with each sample is identified by a lowercase letter.

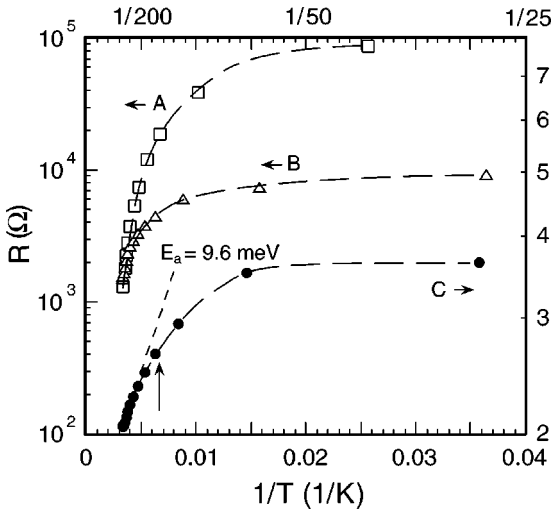

FIG. 5. Logarithm of junction resistance *versus* inverse temperature. Resistance is measured in the vicinity of zero bias ($V \leq 10$ meV). The point at which $1/T = k_B/E_g$ has been indicated on the graph for sample *C*.

Also evident in Fig. 4 is the evolution of the characteristics as the overall magnitude of conductance increases from sample *A* to *D*. This is highlighted by fits with the standard semiclassical double-junction SET (single-electron tunneling) model.[20–22] The fit associated with each sample is identified by a lowercase letter. Also, there are clearly two general types of tunnel systems represented. Samples *A* and *B* exhibit a well-developed gap, whereas samples *C* and *D* exhibit much higher overall tunnel conductance, a significant zero-bias conductance, and a well-suppressed tunnel gap.

As noted above, previous studies (of tunnel systems comprising Pb droplets) have demonstrated that the distribution of single-electron conductance peaks—which are clearly present in other similarly prepared metal-droplet based tunnel structures[16]—was well correlated to droplet diameter distributions.[17] The fits shown in Fig. 4 have included the contribution of a distribution in capacitance, based on the measured droplet-diameter distribution shown in Fig. 3. Excluding this contribution resulted (in all cases) in the appearance of single-electron conductance peaks in the theory that are not present in the data.

The absence of a series of single-electron conductance peaks in the data is consistent with the observed Ni droplet distribution width, $\sigma \sim 100\%$ of the mean droplet diameter, compared to a previously elucidated theoretical result that sets the upper limit for the appearance of conductance peaks at a value of $\sigma \sim 50\%$ of the mean droplet diameter.[22] However, as will be discussed in the following section, the tunneling characteristics and parameters of samples *A* and *B* are consistent with tunneling taking place through a single droplet (and in *C* and *D* on the order of hundreds of droplets). Therefore, while a broad distribution of droplet size would otherwise indicate a smearing and elimination of conductance peaks in all samples, other factors may well be involved.

One such issue is joule heating of droplets as a potential contribution to smearing of the single-electron conductance peaks. Assuming the droplet conduction electrons are strongly coupled to the external environment ($\kappa > 10$ W/cm K), and given typical power levels involved, the expected temperature rise for a given droplet would be in the vicinity of 1 K. Any heating effects beyond this moderate amount would be evident as clear changes in the functional character of the conductance characteristics, or as hystersis in or obvious nonlinear excursions of the current-voltage characteristics, none of which are in any way present. In addition, based on fits both to the temperature dependence of sample resistance, Fig. 5, and fits of the voltage-dependent conductance characteristics to theory, Figs. 6 and 7, the droplets appear to be in thermal equilibrium with the rest of the sample.

In the context of the semiclassical, double-junction model (which appears applicable for samples *A* and *B*) another po-

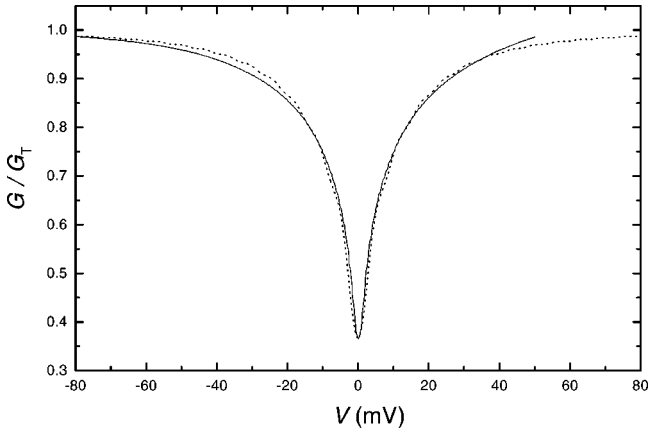

FIG. 6. Comparison of the measured data for sample *C* taken at $T = 4.2$ K (solid line) to that given by the phase correlation theory (dotted line). The data have been normalized to the asymptotic conductance G_T. The theoretical fit was obtained with parameters $T = 4.2$ K, $R_e = 3.8\,\mathrm{k}\Omega$, and $C = 8.0$ aF.

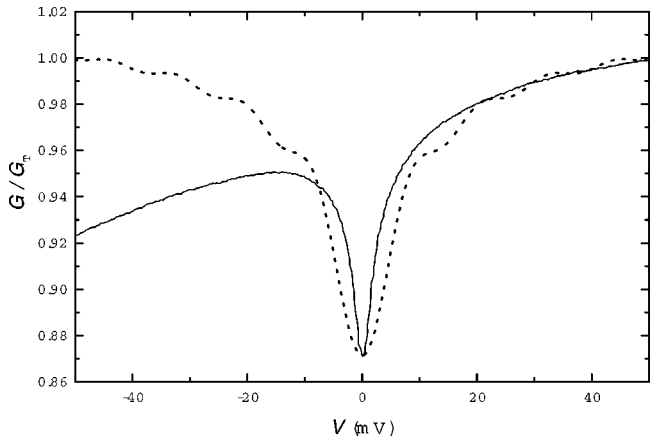

FIG. 7. Comparison of the measured data for sample *D* taken at $T=4.2$ K (solid line) to that given by the phase correlation theory (dotted line). The data have been normalized to the asymptotic conductance G_T. The theoretical fit was obtained with parameters $T=4.2$ K, $R_e=550\,\Omega$, and $C=32$ aF. Barrier asymmetry—the assumed cause of the conductance asymmetry in this very high conductance junction—compromises the fit in the negative bias direction.

tential contributing factor for the absence of conductance peaks is the simple assumption that tunneling to and from individual droplets is symmetric. That is, the product of resistance and capacitance R_1C_1 associated with tunneling onto droplets from one electrode is equal to R_2C_2, the parameters associated with tunneling off of droplets to the other. This appears to be the case, for example, for early tunneling studies of multidroplet systems.[23] Another possibility is the presence of a series array of junctions.[24,25] This is further suggested by microscopic studies of our Ni-droplet films indicating that more than one layer of Ni droplets may exist, especially as film deposition increases.

For the higher conductance systems studied (samples *C* and *D*), we will show that the $P(E)$ theory for single, resistively isolated junctions is in good accord with the measured voltage-dependent conductance curves. This suggests that staircase behavior (and conductance peaks) would be inherently absent here because of the physical characteristics of the systems. Also, since—as we will show—on the order of 10^2 droplets contribute to the total tunnel conductance of these systems, the existence of a distribution of droplet sizes may well contribute to their conductance characteristics.

We note finally that the observed progression from gaplike, parabolic conductance characteristics to a more square-rootlike dependence has experimental precedence in junctions incorporating thin Cr layers, the results for which our data parallel closely.[26,27] Our work with Ni droplets suggests that the broader conductance features that appear in these Cr-based systems are due to the presence of Cr-droplets. These Cr-based junctions also exhibited a magnetic-field-dependent zero-bias anomaly on a 1 meV energy scale, which was absent from our junctions. We note in this regard that the tunneling characteristics of our Ni-droplet tunnel systems were unaffected by the application of magnetic fields up to 9 T at temperatures down to 1.5 K. That is, spin-dependent effects or other zero-bias anomalies appear not to be participating in the tunneling in these systems to the resolution measured.

IV. GAP SUPPRESSION AT HIGH CONDUCTANCE

Besides considerations regarding the absence of staircase behavior, it is clear that the semiclassical (double-junction) approach is generally successful in representing the general features of the low conductance samples *A* and *B*, and fails in fitting the much higher conductance samples *C* and *D* that show a significant zero-bias conductance and lack a fully developed Coulomb gap. This suggests that for samples *A* and *B* the droplets are isolated from the environment by high-barrier height (and high-quality) tunnel barriers separating the droplets from both the Al base- and Ag counterelectrodes, and that for samples *C* and *D*, the physical situation is different. To investigate this, we wish to quantitatively consider the evolution of tunnel conductance associated with individual droplets in the system.

The standard model for the depression of the Coulomb gap starts with a definition of the intrinsic charging energy $E_0=e^2/2C_0$, where C_0 is the geometrical capacitance of either a single ultra-small tunnel junction of capacitance C_0 or a tunnel junction containing an ultra-small island of capacitance C_0. As long as either a single junction, or the nanoelement of a double junction, remains sufficiently isolated from the external environment, the system will exhibit a gaplike blockade of current up to a voltage $V=e/2C_0$ and can also produce a series of steps with a voltage width e/C_0 and current height e/RC_0—the Coulomb staircase (where R is the average slope of the current-voltage characteristics for $V>e/2C_0$).

In the case of a single junction, this isolation can take the form of sufficiently large lead resistances connecting an ultra-small capacitance (area) junction to the external environment and in the case of a double junction, sufficiently large tunneling resistances to and from the internal capacitive element or island. As coupling to the external environment increases, the capacitance is renormalized to a value $C>C_0$, resulting in a reduction of the Coulomb gap and—for double junctions—a smearing of the Coulomb staircase.

We can calculate the unperturbed, geometrical capacitance C_0 and the associated energy $E_0=e^2/2C_0$ for the Ni droplets in our multidroplet tunnel systems. If we model the capacitor as a conducting sphere residing in a infinite dielectric medium, then $C_0=2\pi\epsilon\epsilon_0 D$, where ϵ is the dielectric constant of the medium, $\epsilon_0=8.85\times10^{-12}\,\mathrm{C^2/N\,m^2}$ and D is the diameter of the sphere. For Al_2O_3 $\epsilon=8$ (Refs. 28, 29) implying $E_0=0.36/D$, with E_0 in eV and D in nm. We wish to compare this unperturbed capacitance C_0 with the measured, effective capacitance C of the droplets with tunnel current present.

One measure of the effective capacitance can be gained through the Coulomb blockade energy, established by means of a simple linear extrapolation to $I=0$ of the quasilinear portion of the current-voltage curves. This offset is clearly visible in the data shown in Fig. 1. These values of the gap energy are listed in Table I as E_g along with the associated capacitance $C_g\equiv e^2/2E_g$.

TABLE I. Ni droplet tunnel parameters. D is the average Ni droplet diameter; G is the total dynamic conductance of a multidroplet tunnel system measured at 50 mV bias; $G_D \equiv G/N$ is the average individual droplet conductance in a multidroplet tunnel system with N droplets contributing to the total conductance G; $R(0)$ is the zero-bias resistance of a multidroplet tunnel system; $R_D(0)=NR(0)$ is the average zero-bias resistance associated with an individual conducting droplet; R_e is the environmental resistance for an individual droplet derived from fits with the $P(E)$ theory; $E_0=e^2/2C_0$ is the classical charging energy and C_0 is the geometrical capacitance of an individual droplet; E_g is the gap energy derived from the offset of the current-voltage characteristics, and the capacitance $C_g \equiv e^2/2E_g$; E_a is the activation energy determined by a plot of $\ln R$ *versus* $1/T$ and the capacitance $C_a \equiv e^2/2E_a$; $E_{\rm th}$ is the gap energy derived from $P(E)$ theory and the capacitance $C_{\rm th} \equiv e^2/2E_{\rm th}$. Here, as elsewhere, $G_K \equiv e^2/h \sim 3.874 \times 10^{-5}$ S.

Sample	D (nm)	G (G_K)	G_D (G_K)	N	$R(0)$ (Ω)	$R_D(0)$ (Ω)	R_e (Ω)	E_0 (meV)	E_g (meV)	E_a (meV)	$E_{\rm th}$ (meV)	C_0 (aF)	C_g (aF)	C_a (aF)	$C_{\rm th}$ (aF)
A	1.3	0.19	0.19	1	1.33×10^6	1.33×10^6		139	~150			0.58	~0.53		
B	1.3	4.46	4.46	1	7.11×10^6	7.11×10^6		139	85			0.58	0.94		
C	1.6	4970	18	276	14.0	3860	3800	113	10	9.6	10	0.71	8.0	8.3	8.0
D	1.7	8960	19	472	3.3	1560	550	106	2.5		2.5	0.76	32		32

A separate way to evaluate the effective capacitance is to assume a simple thermal-activation model for the tunneling resistance, $R \propto \exp(E_a/k_BT)$ where E_a is the activation energy associated with removing an electron from a droplet.[30] Shown in Fig. 5 are plots of $\ln R$ *versus* $1/T$. The resistance was obtained by biasing the junction at a small, fixed voltage ($\leqslant 10$ meV) and measuring the current as a function of temperature. For sample *C*, the point at which $1/T = k_E/E_g$ has been indicated on the graph. Above this temperature, there appears to be a well-defined linear regime as is also shown. For samples *A* and *B*, this temperature is higher than room temperature and was not measured, although a small linear region appears to be present for the latter sample. The energy E_a and associated capacitance $C_a = e^2/2E_a$ is also listed in Table I. Sample *D* is absent from this analysis because of problems related to its very low resistance. These data also illustrate generally that the zero-bias conductance in all samples appears to be associated with—or have as a contributing factor—thermally activated tunneling.

The final measure of the Coulomb gap energy and effective droplet capacitance was derived through direct fits to the $G(V)$ characteristics of our tunnel systems with the $P(E)$ (phase correlation) theory.[8,10,11] This theory considers the effects of electromagnetic coupling between ultra-small single-tunnel junctions and their environment through the impedance of the electromagnetic environment, $Z(\omega)$. In this paper, this was modeled by a resistance $R_e = Z(\omega)$. Recently, the effect of R_e on small tunnel junctions has been experimentally investigated.[8,9,31] Measured quantities enter the theory as scaled parameters $a \equiv (\pi/2)R_eG_K$, $\omega_c \equiv 1/R_eC$, and $\Omega_c \equiv \hbar\omega_c/k_BT$.

Figures 6 and 7 show the results of fits (dotted lines) to the measured data for samples *C* and *D* (solid lines). The fit for junction *C* was obtained with $T = 4.2$ K, $R_e = 3.8\,\mathrm{k}\Omega$ and $C = 8.0$ aF, and for sample *D* with $T = 4.2$ K, $R_e = 550\ \Omega$, and $C = 32$ aF. As can be seen from Fig. 6, agreement between theory and experiment is excellent for sample *C* and somewhat compromised in sample *D*, (Fig. 7) because of the asymmetry of the characteristics. Nonetheless, the theoretical values of the capacitance, denoted in Table I as $C_{\rm th}$, for both junctions are in excellent agreement with other measures of the effective capacitance derived from independent means.

Figure 8 shows a global picture of our results in comparison with theory in terms of the reduced capacitance C/C_0 as a function of the tunnel conductance G_T. This includes our work (solid squares, open square, and diamonds) and a compilation of theoretical results[12,32,33] for $E_C/k_BT = 100$, 200, and 500, as indicated on the plot. Since the magnitude of the tunnel conductance is critical in this analysis, it is important to understand its meaning in the context of a multidroplet tunnel system. Here we will assume that, on average, N drop-

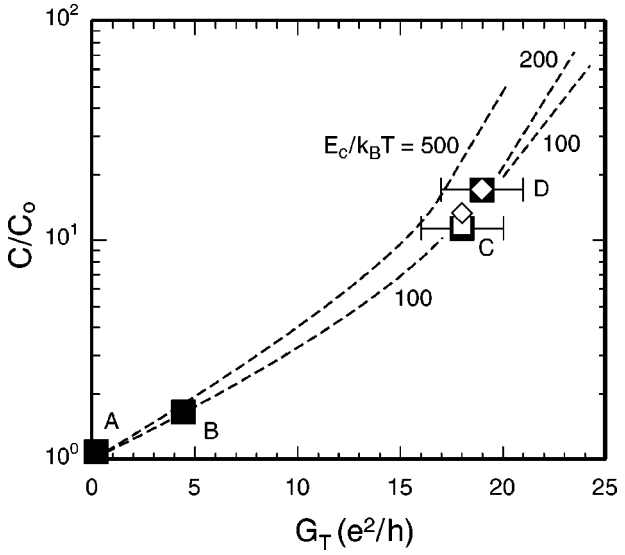

FIG. 8. Reduced capacitance, C/C_0 as a function of tunneling conductance, G_T. C_0 is the geometrical capacitance, and C is the measured capacitance. Included are our results on multidroplet Ni systems derived from: Coulomb blockade effects (solid squares; samples *A*, *B*, *C*, and *D*), thermal activation effects (open square), and theoretical fits with the $P(E)$ theory (diamonds). Also included is a compilation of theoretical results Refs. 12, 32, 33 for $E_C/k_BT = 500$, 200, and 100, as indicated on the plot. For the Ni droplet data, the plotted values of the tunneling conductance $G_T = G_D \equiv G/N$, the total conductance of the multidroplet tunnel system, scaled by the number, N of droplets contributing to the conductance, where N is a whole number providing the best fit to theory. For samples *A*, *B*, *C* and *D*, it is found that $N = 1$, 1, 292, and 498, respectively.

lets contribute to the total conductance of a given tunnel system. This number will be a small fraction of the large number of droplets physically present. We take $N \times G_D \equiv G$ where G_D represents the (average) conductance of each of the *N individual* droplets in the tunnel system contributing to a total conductance G. The total conductance $G \equiv 1/R(50\,\mathrm{mV})$, where $R(50\,\mathrm{mV})$ is the dynamic resistance of a given tunnel system measured at 4.2 K at a dc bias of 50 mV. Plotted values of the tunnel conductance for our samples are taken as $G_T = G_D$ and N is treated as an adjustable integer parameter.

In order to establish N, we rely on the predictions of quantum-fluctuation theory[12,32,33] as shown in Fig. 8. For samples *A* and *B*, the first and second data points in the plot (left to right), $E_g/k_BT = 413$ and 234, respectively. These data are thus in the range covered by the theory. In both cases, best fits to the theory were unambiguously obtained with $N = 1$. That is, it appears that (on average) a single droplet carries all the current in these samples.

For samples *C* and *D* (the third and forth data clusters in the plot) $E_g/k_BT = 28$ and 6.8, respectively. While the reduced energy gap of sample *C* is somewhat outside the parametric range of the theory, it appears to be sufficiently large such that, given the range of variation in the theory with respect to reduced temperature, the two would likely coincide within the error bars shown. Taking a best fit to the data for sample *C* with respect to the theory for $E_C/k_BT = 100$, produces a value of $N = 276$ in this case, which can also be viewed as an upper limit for N. The actual range of N corresponding to the error bars indicated would be $262 < N < 292$. For sample *D*, the value of the reduced gap is sufficiently small as to place it outside current theoretical results. Given this, the data were again fit to the $E_C/k_BT = 100$ theoretical curve to obtain an upper limit for N of 472. For this sample, the range of N corresponding to the error bars indicated would be $448 < N < 498$. In any case, we can certainly conclude that since the total number of droplets comprising a typical tunnel junction (with an area of $\sim 1 \times 1$ mm) is $\sim 10^{11}$, only a tiny fraction of the available droplets appear to contribute substantively to the total conduction of a given multidroplet tunnel system. For samples in the lower conductance regime, it appears that $N = 1$, while in the higher conductance regime $100 < N < 1000$. This is consistent with recent work with granular metal films.[34]

We are left with the question of why the $P(E)$ theory appears to be in excellent agreement with the $G(V)$ data for our (high conductance) multidroplet systems, since the theory is most directly applicable to single, ultra-small tunnel junctions resistively coupled to the environment. Some insight can be gained by comparing the (average) resistance R_D, associated with an individual droplet, to the values of the environmental resistance R_e obtained from fits with the $P(E)$ theory. The simplest physical model of the system would be an array of droplets that on one side see a high-quality barrier (grown on the Al base layer) and on the other, a low-barrier height barrier or one compromised by pinholes, etc., which serves as a resistive coupling element. This situation is similar to nanowire junction arrays[35] that also show good correspondence with the $P(E)$ theory. For sample *D*, the total resistance predicted for each droplet in the system at high bias, $R_D = 1/G_D = 1360\,\Omega$, compared to a parametric value of $R_e = 550\,\Omega$ used in the theoretical fit to the data. (Note that values of G_D listed in Table I are in units of $G_K \equiv e^2/h$.) Since we measure the total resistance of a system, this is consistent with a picture of a droplet with an intrinsic (high-bias) tunnel resistance of 810 Ω (to the base electrode) in series with a resistance $R_e = 550\,\Omega$ (coupled to the counter electrode). Values of R_e in this range are also generally consistent with results for lithographically produced junction arrays with parametric coupling resistances of similar magnitude.[36]

For sample *C*, however, the high-bias resistance $R_D = 1/G_D = 1430\,\Omega$, is smaller than the value of the environmental resistance $R_e = 3800\,\Omega$ used in the theoretical fit to the data. Perhaps coincidentally, this value of R_e is close to the zero-bias resistance of the system that here is $R_D(0) = 3860\,\Omega$. Since $R_D = 1/G_D = N/G$ is proportional to the value of N assigned to the system, one possibility is that this value is too small. However, the variation in N allowed for in fits to the theory (see Fig. 8) amounts to approximately 10% and would not be enough to account for this situation. It appears that in this case, it is the zero-bias resistance of the system that governs the resistive isolation of the droplet. This suggests the presence of nontunneling (resistive) in one or both barriers adjacent to the droplets that act as the parametric equivalent of environmental resistors.

V. CONCLUSION

In conclusion, we have prepared systems containing ultrasmall N droplets. These systems have allowed us to systematically explore the increase in effective junction capacitance as a function of junction conductance into the high conductance regime in multiple-droplet tunnel systems. We have successfully modeled our high conductance junctions with the $P(E)$ (phase correlation) theory. Results for our high conductance samples suggest that these junctions can be modeled as comprising semi-isolated droplets with a resistive coupling to the external environment (single junctions). A result from this paper is a measure of the number of droplets participating in the tunneling conduction. For systems in the low conductance regime where the individual-droplet conductance is in the range of $0.2G_K < G_D < 4.5G_K$, the number of droplets contributing to the total conductance of the system, $N = 1$. This means that a *single* droplet carries the entire current in these systems. In the high conductance regime where the individual-droplet conductance G_D is $18-19\,G_K$, the number of droplets contributing to the total conductance of the system N is found to be 276 and 472, respectively, for the systems studied.

ACKNOWLEDGMENTS

The authors wish to thank T. Cosel for transmission electron micrographs of Ni droplet samples. One of us (Sh.F.) wishes to thank J. P. Pekola for many insightful discussions on this work. We also gratefully acknowledge support of this work by the Department of Energy, Division of Material Sciences, through DE-FG02-88ER45373.

*Email address: ruggiero.1@nd.edu; www.science.nd.edu/physics/faculty/ruggiero.html

[1] G. Schön and A. Zaikin, Phys. Rep. **198**, 237 (1990).
[2] D. Averin and K. Likharev, in *Mesoscopic Phenomena in Solids*, edited by B. Altshuler, P. Lee, and R. Webb (Elsevier, Amsterdam, 1991), p. 173.
[3] *Single Charge Tunneling*, Vol. 294 of *NATO Advanced Studies Institute Series*, edited by H. Grabert and M. Devoret (Plenum Press, New York, 1992).
[4] *Mesoscopic Superconductivity* (1994), Proceedings of the NATO ARW edited by F. Hekking, G. Schön, and D. Averin [Physica B **230**, 201 (1994)].
[5] P. Joyez, V. Bouchiat, D. Esteve, C. Urbina, and M. Devoret, Phys. Rev. Lett. **79**, 1349 (1997).
[6] S. Maurer, S. Patel, C. Marcus, C. Duruoz, and J. J. S. Harris, Phys. Rev. Lett. **83**, 1403 (1999).
[7] G. Göppert, H. Grabert, and C. Beck, Europhys. Lett. **45**, 249 (1999).
[8] S. Farhangfar, J. Toppari, Y. A. Pashkin, A. Manninen, and J. Pekola, Europhys. Lett. **43**, 59 (1998).
[9] P. Joyez, D. Esteve, and M. Devoret, Phys. Rev. Lett. **80**, 1956 (1998).
[10] M. Devoret, D. Esteve, H. Grabert, G.-L. Ingold, H. Pothier, and C. Urbina, Phys. Rev. Lett. **64**, 1824 (1990).
[11] G.-L. Ingold and Y. Nazarov, *Vol. 294 of NATO Advanced Studies Institute Series B: Physics*, edited by H. Grabert and M. Devoret (Plenum, New York, 1992), pp. 197–202.
[12] D. Golubev, J. Konig, H. Schoeller, G. Schön, and A. Zaikin, Phys. Rev. B **56**, 15 782 (1997).
[13] X. Wang and K. Chao, Phys. Rev. B **56**, 12 404 (1997).
[14] G. Göppert, X. Wang, and H. Grabert, Phys. Rev. B **55**, R10 213 (1997).
[15] G. Göppert, H. Grabert, N. Prokof'ev, and B. Svistunov, Phys. Rev. Lett. **81**, 2324 (1998).
[16] J. Barner and S. Ruggiero, Phys. Rev. Lett. **59**, 807 (1987).
[17] S. Ruggiero and J. Barner, Z. Phys. B: Condens. Matter **85**, 333 (1991).
[18] J. B. Barner, Dissertation, University of Notre Dame, 1990.
[19] D. W. Pashley, M. J. Stowell, M. H. Jacobs, and T. J. Law, Philos. Mag. **10**, 127 (1964).
[20] M. Amman, R. Wilkins, E. Ben-Jacob, P. Maker, and R. Jaklevic, Phys. Rev. B **43**, 1146 (1991).
[21] A. Hanna and M. Tinkham, Phys. Rev. B **44**, 5919 (1991).
[22] K. Mullen, E. Ben-Jacob, R. Jaklevic, and Z. Schuss, Phys. Rev. B **37**, 98 (1988).
[23] I. Giaever and H. Zeller, Phys. Rev. Lett. **20**, 1504 (1968).
[24] K. Likharev, N. Bakhvalov, G. Kazacha, and S. Serdyukova, IEEE Trans. Magn. **25**, 1436 (1989).
[25] M. Amman, E. Ben-Jacob, and K. Mullen, Phys. Lett. A **142**, 431 (1989).
[26] F. Mezei, Phys. Lett. **25A**, 534 (1967).
[27] L. Shen and J. Rowell, Phys. Rev. **165**, 566 (1968).
[28] E. Schabowska and J. Szczezeklic, Thin Solid Films **75**, 177 (1981).
[29] W. J. Bernard and J. W. Cook, J. Electrochem. Soc. **106**, 2539 (1963).
[30] K. Inomata and Y. Saito, Appl. Phys. Lett. **73**, 1143 (1998).
[31] P. Wahlgren, P. Delsing, T. Claeson, and D. Haviland, Phys. Rev. B **57**, 2375 (1998).
[32] W. Hofstetter and W. Zwerger, Phys. Rev. Lett. **78**, 3737 (1997).
[33] X. Wang and H. Grabert, Phys. Rev. B **53**, 12 621 (1996).
[34] Y. Inoue, M. Inata, M. Fujii, S. Hayashi, and K. Yamamoto, Thin Solid Films **349**, 289 (1999).
[35] D. Davydov, J. Haruyama, D. Routkevitch, B. Statt, D. Ellis, M. Moskovits, and J. Xu, Phys. Rev. B **57**, 13 550 (1998).
[36] J. Pekola, L. Taskinen, and S. Farhangfar, Appl. Phys. Lett. **76**, 3747 (2000).